Available online at www.sciencedirect.com
ScienceDirect
International Journal of Heat and Mass Transfer 50 (2007) 3701–3717
International Journal of HEAT and MASS TRANSFER
www.elsevier.com/locate/ijhmt

# Buoyancy-aided/opposed convection heat transfer for unsteady turbulent flow across a square cylinder in a vertical channel

Shiang-Wuu Perng [a], Horng-Wen Wu [b,*]

[a] Department of Accounting Information, Kun Shan University, No. 949, Da Wan Road, Yung-Kang City, Tainan Hsien 710, Taiwan, ROC
[b] Department of Systems and Naval Mechatronic Engineering, National Cheng Kung University, Tainan, Taiwan, ROC

Received 5 January 2007; received in revised form 16 February 2007

**Abstract**

The Large Eddy Simulation (LES) and SIMPLE-C method coupled with preconditioned conjugate gradient methods have been employed to study the effect of aiding/opposing buoyancy on the turbulent flow field and heat transfer across a square cylinder in a vertical channel. The level of wall-confinement (blockage ratio of 10%, 30% and 50%) was changed with a constant Reynolds number (5000) under various Richardson numbers (−1 to 1). With increasing blockage ratio, the buoyancy effect is becoming weaker on the Nusselt number for the square cylinder. The turbulent heat transfer past the square cylinder can be improved by increasing the blockage ratio.


*Keywords:* LES; Heat transfer; Buoyancy; Blockage ratio; Vortex shedding; Square cylinder

## 1. Introduction

Unsteady natural convection flow past bluff bodies in vertical channels has been a subject of numerous engineering applications such as heat exchangers, natural circulation boilers, nuclear reactors, solar heating systems, dry cooling towers, and cooling of electronic equipment. The designs of the configurations require a thorough understanding of the influence of the unsteady vortex structure on the heat transfer and flow field. Most previous studies were focused on circular cylinders placed in a free-stream flow [1,2]. However, flow around the square cylinder is also an important fundamental problem of engineering interest and is investigated here.

Most of the previous heat transfer studies on channel-confined flow across a square cylinder were considered as the forced convection problem [3–5]. Rahbana and Hadi-Moghaddam [6] investigated numerically the unsteady laminar flow past a heated square cylinder mounted inside a plane channel with a blockage ratio of 1/8. Valencia [7] employed the $\kappa-\varepsilon$ turbulence model to study the heat transfer and friction in a channel with a mounted square bar of different sizes detached from the channel wall.

Although many papers have been conducted on the channel-confined flow past a square cylinder for forced convection, there are few studies on natural convection. Chang and Sa [8] numerically studied the effect of the buoyancy on the flow past a hot/cold circular cylinder, at $Re = 100$ for $-1 \leqslant Ri \leqslant 1$ and found suppression of vortex shedding at a critical $Ri$ of 0.15. Sharma and Eswaran [9] showed the influence of channel-confinement and aiding/opposing buoyancy on the 2D laminar flow and heat transfer across a square cylinder. Ho et al. [10] investigated the aiding buoyancy in the steady flow regime with uniform inlet velocity profile for both unconfined and channel-confined upward flow across circular cylinder at $Re = 20, 40$ and $60, 0 \leqslant Ri \leqslant 4$, and blockage ratio of 50%, 25%, 16.67%, and 0%. These above cited papers investigated the laminar flow across a cylinder in a channel with various parameter $Ri$ and blockage ratios, but there are still many other engineering problems involving the turbulent flow. Examining the effect of the buoyancy and the blockage

* Corresponding author. Tel.: +886 6 274 7018x223; fax: +886 6 274 7019.
*E-mail address:* z7708033@email.ncku.edu.tw (H.-W. Wu).

0017-9310/$ - see front matter © 2007 Elsevier Ltd. All rights reserved.
doi:10.1016/j.ijheatmasstransfer.2007.02.026

**Nomenclature**

| | |
|---|---|
| $B$ | width of the square cylinder |
| $C_K$ | SGS model variable in LES ($C_K = 0.094$) |
| $C_L$ | lift coefficient ($F_L/\frac{1}{2}\rho v_\infty^2 B$) |
| $C_S$ | Smagorinsky constant |
| $D$ | hydraulic diameter of channel ($D = 2H$) |
| $dA$ | surface area increment along the square cylinder |
| $E_{SGS}$ | dimensionless subgrid-scale kinetic energy |
| $f_S$ | frequency of the vortex shedding |
| $f_\mu$ | Van Driest wall damping function $\left(\left[1-\exp\left(-y_n^+/25\right)^3\right]^{1/2}\right)$ |
| $G$ | grid filter function |
| $Gr$ | Grashof number ($g\beta(T_w^* - T_\infty^*)B^3/v^2$) |
| $H$ | channel width |
| $l$ | dimensionless characteristic length scale |
| $L$ | channel length |
| $L_D$ | distance between top surface of cylinder and exit plane |
| $L_U$ | distance between inlet plane and bottom surface of cylinder |
| $n$ | normal vector |
| Nu | Nusselt number ($\partial\theta/\partial n$) |
| $[Nu]$ | time-mean Nusselt number ($\int Nu dt/\int dt$) |
| $\langle Nu\rangle$ | surface-mean Nusselt number ($\int Nu dA/\int dA$) |
| $P$ | dimensionless static pressure ($P_S/\rho v_\infty^2$) |
| $P_S$ | static pressure |
| $P^*$ | summation of $\bar{P}$ and $\frac{2}{3}E_{SGS}$ |
| $Pr$ | Prandtl number ($v/\lambda$) |
| $Pr_T$ | turbulent Prandtl number |
| $q$ | constant heat flux in Lockett's reference [26] |
| $R$ | computational domain |
| $Re$ | Reynolds number based on channel height ($v_\infty B/v$) |
| $Re_D$ | Reynolds number based on twice channel height ($v_\infty D/v$) |
| $Re_{eff}$ | effective Reynolds number |
| $Re_{SGS}$ | SGS Reynolds number |
| $Ri$ | Richardson number ($Ri = Gr/Re^2$) |
| $Sr$ | Strouhal number ($Sr = h\cdot f_S/v_\infty$) |
| $S_{ij}$ | strain rate tensor of the flow field $\left(S_{ij} = \frac{1}{2}\left(\frac{\partial u_i}{\partial x_j}+\frac{\partial u_j}{\partial x_i}\right)\right)$ |
| $\lvert\bar{S}\rvert$ | mean strain $\left(\lvert\bar{S}\rvert = \sqrt{2\bar{S}_{ij}\bar{S}_{ij}}\right)$ |
| $S_\Phi$ | source term for variable |
| $T^*$ | temperature |
| $T_\infty^*$ | uniform inlet temperature |
| $t$ | dimensionless time ($t^*/(B/v_\infty)$) |
| $t^*$ | time |
| $\Delta t$ | dimensionless time interval |
| $u$, $v$ | dimensionless velocity components ($u = u^*/v_\infty$, $v = v^*/v_\infty$) |
| $u_\tau$ | friction velocity $\left(u_\tau \equiv \sqrt{\frac{\tau_w}{\rho}}\right)$ |
| $u^*, v^*$ | velocity components |
| $v_\infty$ | uniform inlet velocity |
| $w$ | height of square rib in Lockett's reference [26] |
| $x$, $y$ | dimensionless $x^*$, $y^*$ coordinates ($x = x^*/B, y = y^*/B$) |
| $x^*, y^*$ | physical coordinates |
| $x_i$ | Cartesian coordinates ($i = 1$ for $x$-coordinate; $i = 2$ for $y$-coordinate) |
| $y_w$ | near-wall distance |
| $y_n^+$ | dimensionless distance from the wall $\left(y_n^+ \equiv \frac{y_w u_\tau}{v}\right)$ |

*Greek symbols*

| | |
|---|---|
| $\bar{\Delta}$ | grid filter width |
| $\Phi$ | general dependent flow variable |
| $\Phi'$ | subgrid-scale component of $\Phi$ |
| $\Gamma_\Phi$ | diffusion coefficient |
| $\lambda$ | thermal diffusivity |
| $v$ | laminar kinematic viscosity |
| $\rho$ | density |
| $\tau_w$ | wall shear stress |
| $\theta$ | dimensionless temperature $\left((T^* - T_\infty^*)/(T_w^* - T_\infty^*)\right)$ |
| $\xi$ | natural coordinate in computational domain |
| $\zeta$ | dimensionless distance along ribbed wall in Lockett's reference [26] |

*Superscript*

| | |
|---|---|
| – | spatial grid filter indication |

*Subscripts*

| | |
|---|---|
| $i, j$ | indication of components |
| w | indication of wall boundary |

ratio on the turbulent flow and heat transfer past a square cylinder in a channel is a motivation to us from practical consideration. The purpose of this study is to quantify the influence of the channel-confinement of various degrees for a square cylinder on the flow field and heat transfer under various Richardson numbers.

The Reynolds-averaged simulations require a fine grid to resolve the regions of rapid variations. Given the complexity of the Reynolds-averaged simulations, a Large Eddy Simulation (LES) might actually be simpler, shorter in execution and more accurate. In the Reynolds-averaged simulations the length scales of the turbulence usually are much larger than the grid spacing. The Reynolds-averaged simulations only reveal unsteady motions of scales larger than the model's turbulence scale. Besides, the eddy viscosity is obtained from the length scale of the smallest eddy in

the turbulent models. Therefore, the volume-average filtered Navier–Stokes equations are fairly insensitive to the turbulent models in a Large Eddy Simulation (LES) [11]. The turbulent, vortex shedding flow a long square cylinder, which is two-dimensional in the mean, is simulated by Large Eddy Simulation (LES). When the mean flow is two-dimensional, it is common for engineering problems to perform two-dimensional computation, because the CPU time is then reduced greatly in comparison with three-dimensional computation [12].

In this study, the SIMPLE-C method [13] and LES [14] are employed to investigate the influence of blockage ratio and aiding/opposing buoyancy on the turbulent flow and heat transfer across a square cylinder in a vertical channel. The transient term is discretized with Second-order Backward Euler (SBE) method [15] to remove stability restrictions and the convection terms with Extended Linear Upwind Differencing (ELUD) method (third-order scheme) [16] to avoid severe oscillations. Also, iterative solution methods based on the preconditioned conjugate gradient method [17,18] were incorporated into the solving process with second-order time advancement.

The SIMPLE-C method coupling with the above discretization techniques generally requires less computer storage and computation time than the conventional SIMPLE method. The results of this paper may be of interest to engineers attempting to develop thermal control of heat exchangers or electronic devices and to researchers interested in the turbulent flow-modification and heat transfer across a square cylinder under aiding/opposing buoyancy in a vertical channel.

## 2. Mathematical formulation

The two-dimensional flow geometries and the relevant dimensions considered for the analysis are schematically shown in Fig. 1. The unsteady, turbulent, and incompressible flow is assumed to investigate the mixed convection heat transfer over a square cylinder mounted in the center line of the vertical channel. The calculation of the thermal turbulent flow field with the Large Eddy Simulation (LES) requires obtaining the solution of the governing equations.

The flow variables in LES are decomposed into a large-scale component, denoted by an overbar, and a

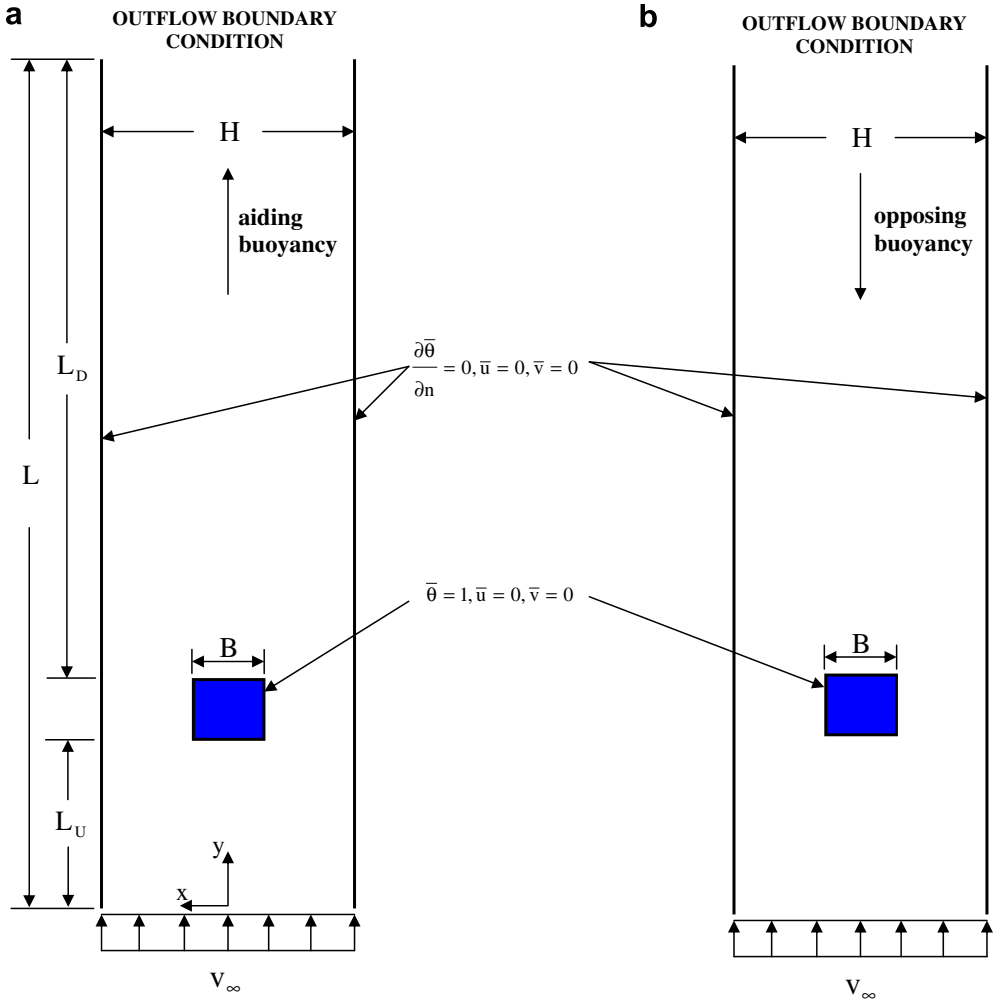


Fig. 1. The geometries considered here: (a) under aiding buoyancy and (b) under opposing buoyancy in a vertical channel.

subgrid-scale component. The large-scale component is defined by the following operation:

$$\overline{\Phi}(x_i,t)=\int_R G(x_i-\xi)\Phi(\xi)\mathrm{d}\xi,\quad \Phi=\overline{\Phi}+\Phi' \tag{1}$$

where the integral is extended over the entire domain $R$, and $G$ is the grid filter function. The length associated with $G$ is the grid filter width $\overline{\Delta}$.

The dimensionless transport equations representing the conservation of mass, momentum and thermal energy are cast into a general form of time-dependent and two-dimensional Cartesian coordinates, and the dimensionless governing transport equations are in terms of being filtered by a simple volume-averaged box filter under the Boussineq approximation [19] as follows:

$$\frac{\partial\overline{\Phi}}{\partial t}+\frac{\partial}{\partial x}\left(\bar{u}\overline{\Phi}\right)+\frac{\partial}{\partial y}\left(\bar{v}\overline{\Phi}\right)=\frac{\partial}{\partial x}\left(\Gamma_\Phi\frac{\partial\overline{\Phi}}{\partial x}\right)+\frac{\partial}{\partial y}\left(\Gamma_\Phi\frac{\partial\overline{\Phi}}{\partial y}\right)+S_\Phi(x,y) \tag{2}$$

where $\overline{\Phi}$ represents one of the following entities: 1, $u$, $v$, or $\theta$, in which the dependent dimensionless variables are velocity components $u$, $v$, and temperature $\theta$. Also, $t$ stands for dimensionless time, $\Gamma_\Phi$ for the corresponding effective diffusion, and $S_\Phi$ for the source term. The corresponding expressions of $\Gamma_\Phi$ and $S_\Phi$ are given in Table 1. In Eq. (2), the notation $\overline{\Phi}=1$ denotes the continuity equation.

In Table 1, $Re_{\mathrm{SGS}}$ is the subgrid-scale (SGS) Reynolds number, $Re_{\mathrm{eff}}$ is the effective Reynolds number, $P$ is the static pressure, and $E_{\mathrm{SGS}}$ is the SGS turbulent kinetic energy.

### 2.1. Turbulence modeling

Initial runs of the present research revealed that the conventional Smagorinsky model [22] did not generate appropriate levels of eddy viscosity in the complex physical domain. For the reason, the Van Driest wall damping SGS model [23] is used here as follows:

$$\frac{1}{Re_{\mathrm{SGS}}}=l^2\times\sqrt{2\times\widetilde{S}_{ij}\widetilde{S}_{ij}},\ l=C_{\mathrm{S}}f_\mu\overline{\Delta},\ \ f_\mu=\left[1-\exp\left(-y_n^+/25\right)^3\right]^{1/2} \tag{3}$$

where $l$ is a dimensionless characteristic length scale of small eddies, $C_{\mathrm{S}}$ is equal to 0.15 [12], $f_\mu$ is the Van Driest wall damping function, and $y_{\mathrm{n}}^+\equiv y_{\mathrm{w}}u_\tau/\nu$. The Van Driest wall damping function is used to account for the near-wall effect. $\overline{S}_{ij}$ is a dimensionless strain rate tensor of the filtered flow field.

$$\overline{S}_{ij}=\frac{1}{2}\left(\frac{\partial\bar{u}_i}{\partial x_j}+\frac{\partial\bar{u}_j}{\partial x_i}\right),\ \ |\overline{S}|=\left(2\times\overline{S}_{ij}\overline{S}_{ij}\right)^{0.5} \tag{4}$$

### 2.2. Computational domain, boundary and initial conditions

The computational domains are shown in Fig. 1 for a fixed two-dimensional square cylinder with side $B$ (which is also the non-dimensional length scale) in a vertical channel. The geometrical relations in these cases are set forth: $L/B=26$, $L_{\mathrm{U}}/B=8.5$, $L_{\mathrm{D}}/B=16.5$ and different $B/H$ values (blockage ratios of 10%, 30% and 50%). The stream-wise and cross-stream directions are parallel to the coordinate axes $y$ and $x$.

Flow and temperature fields in the near-wall region are matched to the boundary layer models. According to the research of Werner and Wengle [24], we assume that the instantaneous tangential velocity inside the first grid cell is in phase with the instantaneous wall shear stress and that a linear or 1/7 power-law distribution of the instantaneous velocity is used:

$$\frac{\bar{u}}{u_\tau}=y_{\mathrm{n}}^+\quad(\text{when } y_{\mathrm{n}}^+\leqslant 11.81) \tag{5}$$

$$\frac{\bar{u}}{u_\tau}=8.3y_{\mathrm{n}}^{+1/7}\quad(\text{when } y_{\mathrm{n}}^+>11.81) \tag{6}$$

where $u_\tau$ is the friction velocity and $y_{\mathrm{n}}^+$ the dimensionless distance from the wall. Thermal near-wall boundary conditions were also implemented to be coherent with the above instantaneous velocity ones. They were based on the universal temperature profiles of Jayatilleke [25] for a Prandtl number of 0.71.

All cases have the same external boundary conditions; uniform inflow with $\bar{u}=0$, $\bar{v}=1$; no-slip boundary conditions $\bar{u}=0$ and $\bar{v}=0$ on the two channel walls; and a standard outflow condition across the exit plane; and $\partial\bar{\theta}/\partial n=0$ along the two channel walls. A no-slip surface $\bar{u}=0$ and $\bar{v}=0$ is specified on the square cylinder surfaces with constant temperature $\bar{\theta}=1$. The initial conditions are $\bar{u}=\bar{v}=\bar{\theta}=0$ in the computational domain for $t=0$.

Table 1
Definition of $\Phi$, $\Gamma_\Phi$ and $S_\Phi$

| $\Phi$ | $\Gamma_\Phi$ | $S_\Phi$ |
|---|---|---|
| 1 | 0 | 0 |
| $u$ | $\frac{1}{Re_{\mathrm{eff}}}$ | $-\frac{\partial P^*}{\partial x}+\frac{\partial}{\partial y}\left(\frac{1}{Re_{\mathrm{eff}}}\frac{\partial\bar{v}}{\partial x}\right)+\frac{\partial}{\partial x}\left(\frac{1}{Re_{\mathrm{eff}}}\frac{\partial\bar{u}}{\partial x}\right)$ |
| $v$ | $\frac{1}{Re_{\mathrm{eff}}}$ | $-\frac{\partial P^*}{\partial y}+\frac{\partial}{\partial y}\left(\frac{1}{Re_{\mathrm{eff}}}\frac{\partial\bar{v}}{\partial y}\right)+\frac{\partial}{\partial x}\left(\frac{1}{Re_{\mathrm{eff}}}\frac{\partial\bar{u}}{\partial y}\right)+Ri\bar{\theta}$ |
| $\theta$ | $\frac{1}{PrRe}+\frac{1}{Pr_{\mathrm{T}}Re_{\mathrm{SGS}}}$ | 0 |

*Note:*
$\frac{1}{Re_{\mathrm{eff}}}=\frac{1}{Re}+\frac{1}{Re_{\mathrm{SGS}}}$, $P^*=\bar{P}+\frac{2}{3}E_{\mathrm{SGS}}$, $E_{\mathrm{SGS}}=\left(\frac{1}{C_K\overline{\Delta}}\cdot\frac{1}{Re_{\mathrm{SGS}}}\right)^2$,
$C_{\mathrm{K}}=0.094$ [20], $Pr_{\mathrm{T}}=0.9$ [21].

## 3. Numerical methods

The SIMPLE-C algorithm with the control volume approach is adopted to derive the discretized forms of all

transport equations arranged into transient, diffusion, convection, and source terms. By adopting an Extended Linear Upwind Differencing (ELUD) to discretize the convective terms and a Second-order Backward Euler (SBE) to discretize the transient term, we may derive the fully discretized equations by means of control-volume method. These discretized equations are easily implemented into the SIMPLE-C algorithm.

The iterative solution methods based on the preconditioned conjugate gradient method are incorporated into this code. In this paper, the ICCG method [17] is used for the Poisson pressure correction equation, and the ILU-BiCG method [18] for the equations of $u$, $v$, and $\theta$. The dimensionless time step was tested to be set as 0.001 for the calculations of unsteady flow and heat transfer across a square cylinder in a vertical channel under aiding/opposing buoyancy. The calculations were terminated when the mass residual is less than $10^{-4}$ and the solution for nodal velocity components varied less than $10^{-5}$ between two consecutive iterations.

## 4. Results and discussion

### 4.1. Model validation

In this study, the above mentioned numerical methods are applied to investigate the unsteady turbulent flow and mixed convection heat transfer across a square cylinder in a vertical channel. The following range of parameters are considered: blockage ratio, $B/H = 10\%$, 30% and 50%, and Richardson number is considered as $-1$ to 1 (positive value represents the aiding buoyancy and negative value opposing buoyancy) when $Re$ is kept constant at 5000 and $Pr$ as 0.71. All the calculations have been performed by using a PENTIUM 4 3.0G PC. After a series of grid independent test runs ($40 \times 150$; $65 \times 200$; $80 \times 350$; $100 \times 420$, the former is in $x$-axis and the latter is in $y$-axis), the mesh ($80 \times 350$) was chosen in all cases from the sensitivity results as shown in Fig. 2a. The time step size is adjusted in this numerical code from stability and accuracy criteria with the initial time step size given as an input. The four time steps 0.0005, 0.001, 0.002, and 0.004 were chosen to test the time step size sensitivity. As the results were compared in Fig. 2b, the time increment $\Delta t$ could be set as 0.001 for the calculations of unsteady turbulent flow and heat transfer across a square cylinder in a vertical channel. In these calculations for the study, about 300,000 time steps were necessary to obtain reasonably reliable statistics. The computation CPU times were about 117 h 15 min 51 s–120 h 29 min 47 s in all cases.

In order to prove that the program in this paper can handle turbulent flow and heat transfer around the cylinders in the channel, we employ the present method to solve the turbulent flow in the ribbed channel employed in the experiments of Lockett [26]. The ratio of square rib height

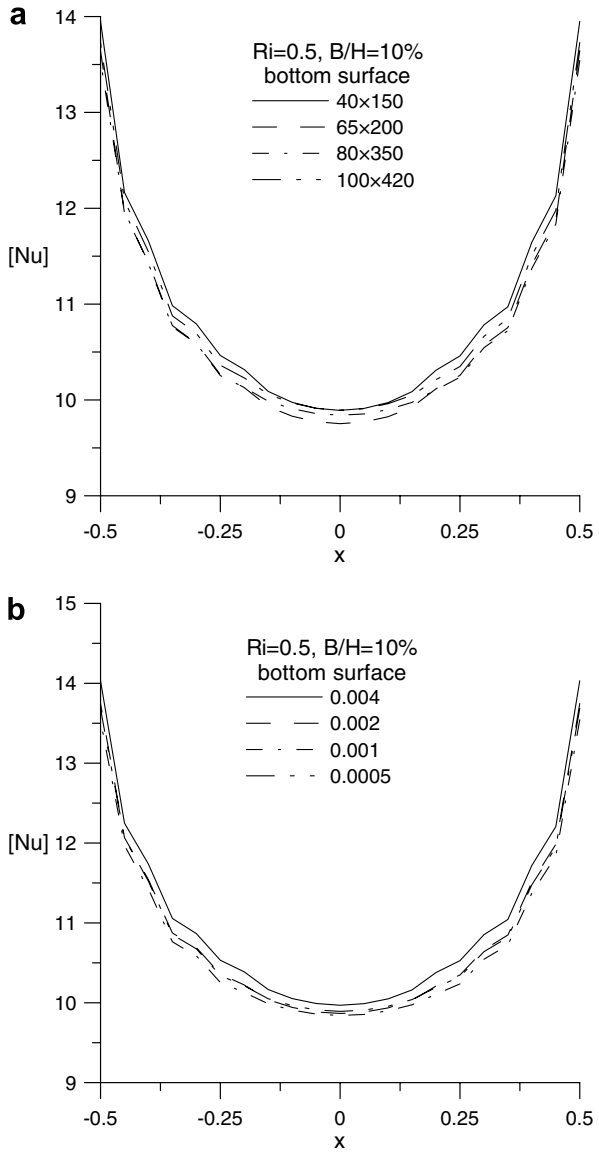


Fig. 2. (a) Grid sensitivity. (b) Time step size sensitivity at $Ri = 0.5$ and $B/H = 10\%$ for time-mean Nusselt number along the bottom surface of square cylinder in the vertical channel.

($w$) to channel height ($w/H$) was 1/9.5, the ratio of channel length to channel height was 8, and $Re_D$ was 30,000 for the ribbed channel in Lockett's experiment. The periodic boundary condition was imposed along the stream-wise direction ($x$). Besides, the bottom wall has a constant heat flux $q$ on the horizontal wall between ribs and a value $q/3$ on each face of a rib while the top wall was adiabatic for the thermal boundary conditions in the ribbed channel. The mesh size employed for the comparison with the references was $96 \times 48$ (along $x$ and $y$ directions). The steady-state solution is obtained by the numerical procedure as mentioned in the previous section. The present predictions for the normalized Nusselt number $Nu/\langle Nu \rangle$ of the bottom wall and rib faces are compared with the numerical results calculated by Ciofalo and Collins [27] and the

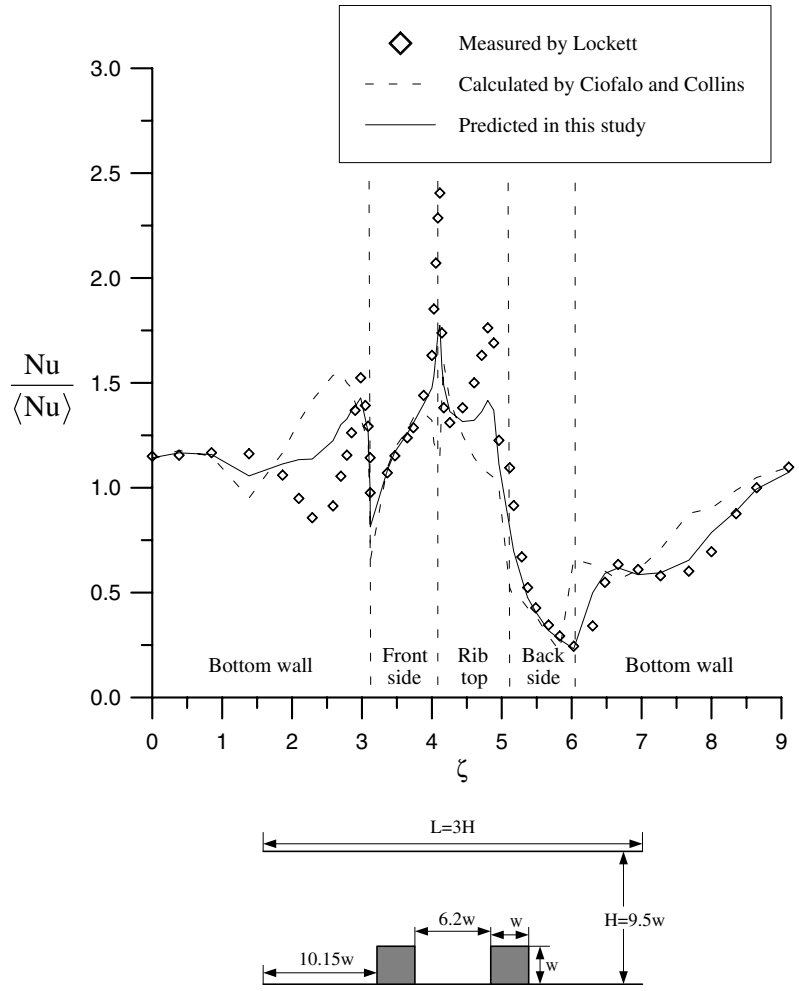


Fig. 3. Comparison the results between the numerical predictions and Lockett's experiment.

experimental results measured by Lockett as shown in Fig. 3. These curves of the present predictions and the references have the same trend with channel length, and the overall relative difference between the curves is less than 2.15%.

### 4.2. Influence of buoyancy

The time-mean Nusselt number will be employed below to realize the turbulent heat transfer characteristics in all cases with various blockage ratios in this study. The time-mean Nusselt number for the square cylinder is calculated in a time interval containing several flow cycles of vortex shedding. In Fig. 4a and c, the local Nusselt number along bottom, left and right surfaces of the square cylinder increases with decreasing *Ri*. On the bottom surface, the maximum local Nusselt number for the square cylinder occurs at the two corners while the minimum value occurs at midpoint of bottom surface ($x = 0$). On the left and right surfaces, the local Nusselt number approximately decreases along the surface under the aiding buoyancy ($Ri = -0.5$ and $-1.0$), but it increases along the surface after $y = 8.9$ under the opposing buoyancy ($Ri > 0$). In Fig. 4b, the local Nusselt number along top surface of the square cylinder increases with an increase in *Ri*. Overall, at $B/H = 10\%$, the influence of aiding buoyancy is prominent on the top surface of the square cylinder, while the opposing buoyancy has obvious effect on the other three surfaces. Similar influence has been observed for the laminar flow in an earlier study [28]. At $B/H = 30\%$ (Fig. 5), the distributions of the local Nusselt number along the square cylinder have the similar profile in the cases at $B/H = 10\%$. There is a difference between $B/H = 10\%$ and $B/H = 30\%$ for the local Nusselt number. In Fig. 5 ($B/H = 30\%$), the buoyancy effect on the local Nusselt number along the bottom surface is weak, and the buoyancy effect on the local Nusselt number along the top, left and right surfaces is becoming less obvious than the $B/H = 10\%$ case. At $B/H = 50\%$ (Fig. 6), the above phenomena is more obvious than the $B/H = 30\%$ case, and especially the buoyancy effect on the local Nusselt number along the bottom, left and right surfaces is almost in vain. From the above statements about the profiles of the local Nusselt number for various $B/H$ and *Ri*

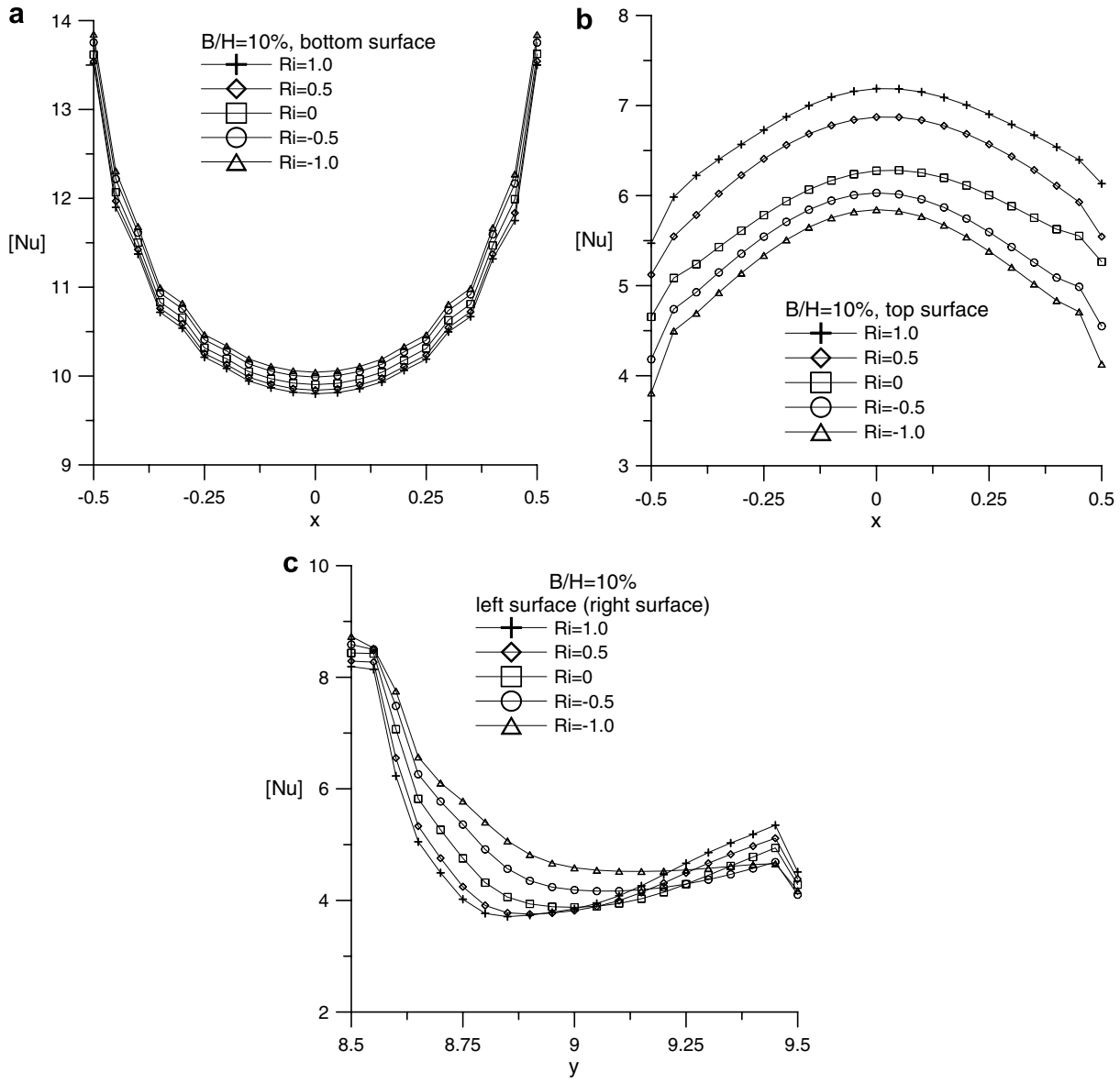


Fig. 4. Time-mean Nusselt number profiles along (a) bottom, (b) top and (c) left (right) surfaces of the square cylinder for $Ri$ values at $B/H = 10\%$.

values, the interaction between the blockage of the square cylinder and the buoyancy has the influence on the heat transfer in a vertical channel. Furthermore, the streamlines for different $B/H$ values ($B/H = 10\%$, 30% and 50%) under the influence of aiding and opposing buoyancy at $Re = 5000$ were presented in Fig. 7 to understand the profiles of Nusselt number. The turbulent flow around the square cylinder placed in the center line of a vertical channel is very complicated since it is defined by stagnation in bottom surface of the square cylinder, separation at the two corners of the bottom surface. Besides, two small re-circulating zones individually are formed along the left and right surfaces of the cylinder, and a vortex shedding generates in the wake region above the top surface. The curvature of the streamline becomes very large locally at the two corners of the bottom surface; this has a high velocity, so the convection heat transfer is large. These re-circulating zones are formed along the top, left and right surfaces of the cylinder, so that the heat is transferred poorly from the re-circulating zone fluid to the mainstream flow. Fig. 7a and b shows that the opposing buoyancy generates a shorter length of the wave flow than the aiding buoyancy; thus, the opposing buoyancy has a smaller Nusselt number on the top surface (Fig. 4b), but the phenomenon in Fig. 7c does not exist because of confinement of the channel wall. Besides, a smaller re-circulating zone generates in the wake region under the opposing buoyancy than the aiding buoyancy as shown in Fig. 7a and b. The strength of shear layer increases and the roll-up process is more activated with increasing cooling of the cylinder because the velocity in the wake region is reduced by the opposing buoyancy of cold air. The above results of the

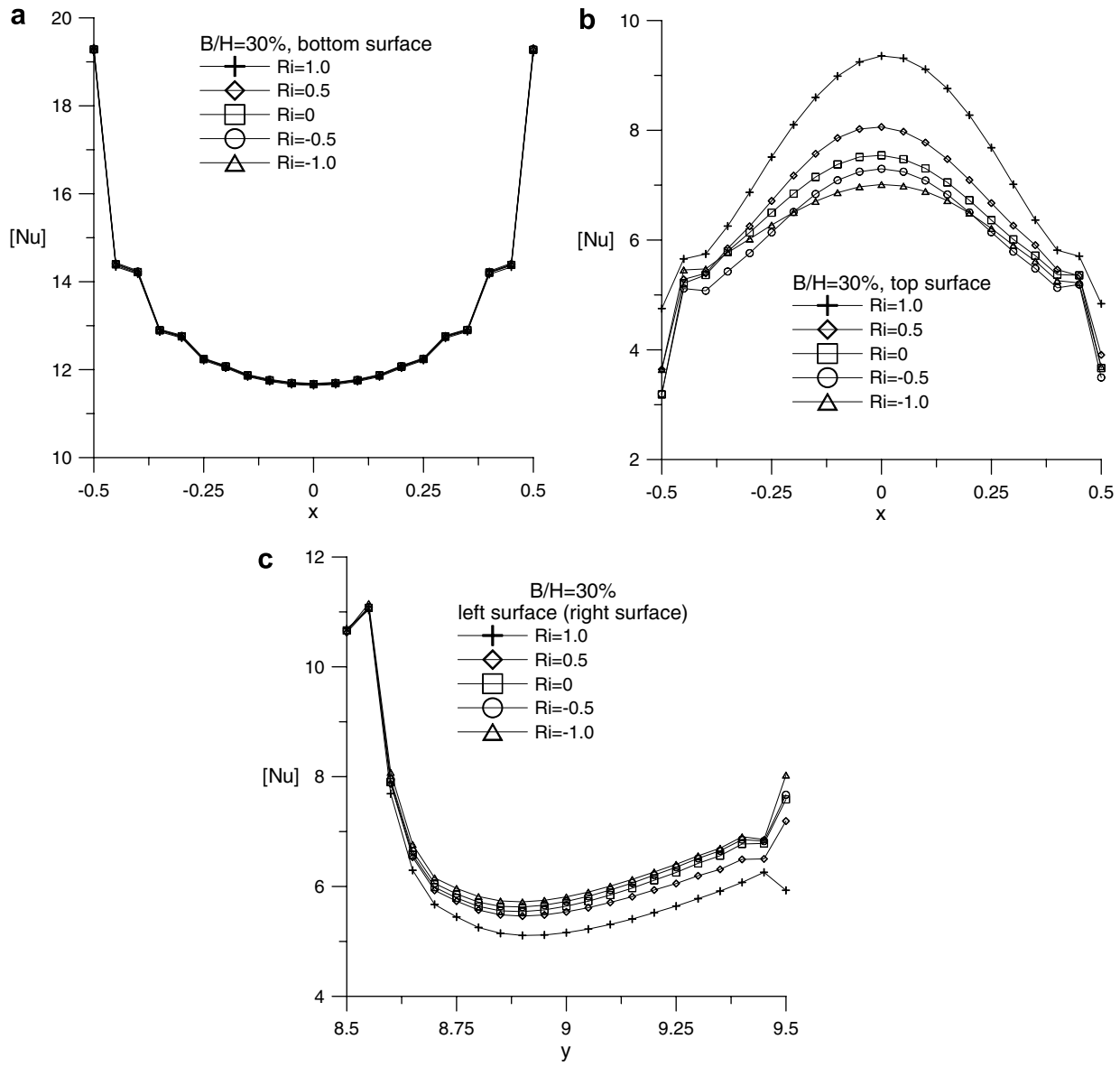


Fig. 5. Time-mean Nusselt number profiles along (a) bottom, (b) top and (c) left (right) surfaces of the square cylinder for $Ri$ values at $B/H = 30\%$.

effect of buoyancy on the cylinder were also mentioned for the laminar flow past a circular cylinder in an earlier study [8]. The reduced velocity in the wake region by the opposing buoyancy gets the poor heat transfer. These results can provide confirmation to the profile of the local Nusselt number along the top surface in Figs. 4b and 5b. Fig. 8 illustrates the isothermal distribution around the square cylinder for the aiding and opposing buoyancy with various $B/H$ values. Closer isothermal lines indicate a higher temperature gradient and accordingly a higher Nusselt number. From Fig. 8, the isothermal lines around the bottom, left and right surfaces separate more under the aiding buoyancy than under the opposing buoyancy, and then the Nusselt number along these surfaces becomes smaller. However, the isothermal lines around the top surface have the opposite tendency.

### 4.3. Influence of confinement of channel wall

The influence of the channel-confinement of various degrees for a square cylinder on the turbulent flow and heat transfer is investigated by letting the parameter $B/H$ (blockage ratio) equal 10%, 30% and 50% in this study. Fig. 9 shows the profile of the local Nusselt number along the cylinder under the aiding buoyancy with various $B/H$. From Fig. 9a and c, the Nusselt number along the bottom and side surfaces increases with increasing $B/H$ value under the aiding buoyancy, especially along the side surfaces, because the fluid is confined by the channel wall. In Fig. 9b, the Nusselt number along the top surface with $B/H = 50\%$ is the minimum among three blockage ratios because of the interaction between the re-circulating zone and the wall-confinement in the wake region. For the

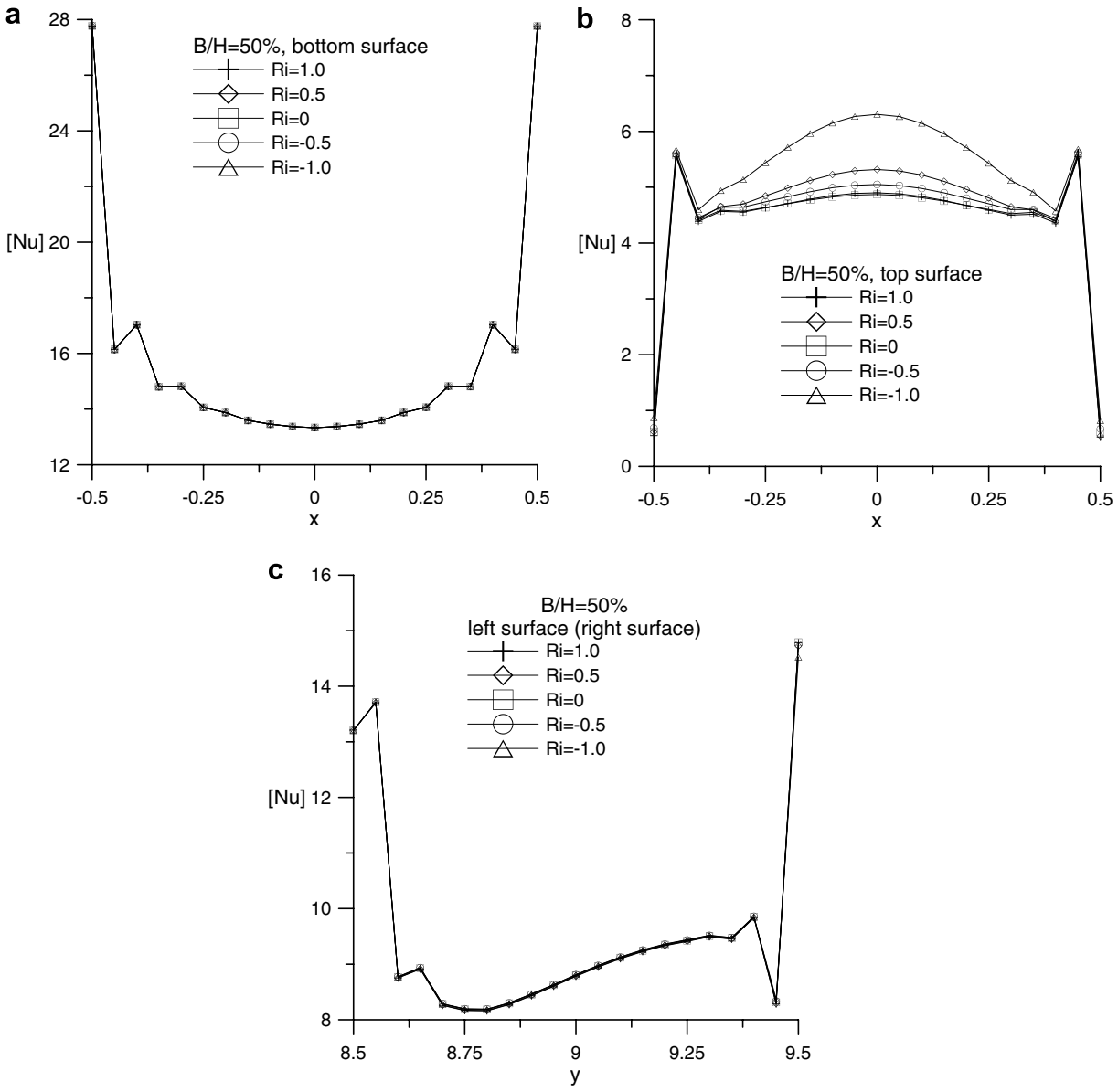


Fig. 6. Time-mean Nusselt number profiles along (a) bottom, (b) top and (c) left (right) surfaces of the square cylinder for $Ri$ values at $B/H = 50\%$.

opposing buoyancy in Fig. 10, the profiles of the Nusselt number along the square cylinder have the same tendency as mentioned in Fig. 9. The streamlines are shown in Fig. 7 to understand the influence of the channel-confinement on the turbulent flow field. With increasing the degree of the channel-confinement from $B/H = 10\%$ to 30%, the channel wall gradually confines the streamlines near the cylinder and an increase in the velocity of the fluid in the wake region enhances the heat transfer from the top surface. However, with a further increase in $B/H$ value, the velocity of the fluid emanating from the gap between the sides faces of the cylinder and the channel wall increases. This flow jets upward to make fluid particles flow into the wake cavity, so the heat transfer from the top face at $B/H = 50\%$ is the most poor between three blockage ratios. From Fig. 7a and (a-1), the streamline along the channel walls has an almost symmetric distribution about the center line of the channel while $B/H$ equals 10%. However, this symmetry disappears while $B/H$ is 30% and 50% as shown in Fig. 7b, (b-1), c and (c-1). Thus, the time-dependent flow motion is only noticeable near the square cylinder and the fluid flow along the channel wall changes nothing for the cylinder at $B/H = 10\%$. While the blockage ratio increases to be 30% and 50%, the flow along the channel wall becomes unsteady and some re-circulating zones occur along the channel wall. From Fig. 8, the isothermal lines around the bottom and side surfaces become closer with increasing $B/H$ value, and then the Nusselt number along the bottom and side surfaces increases.

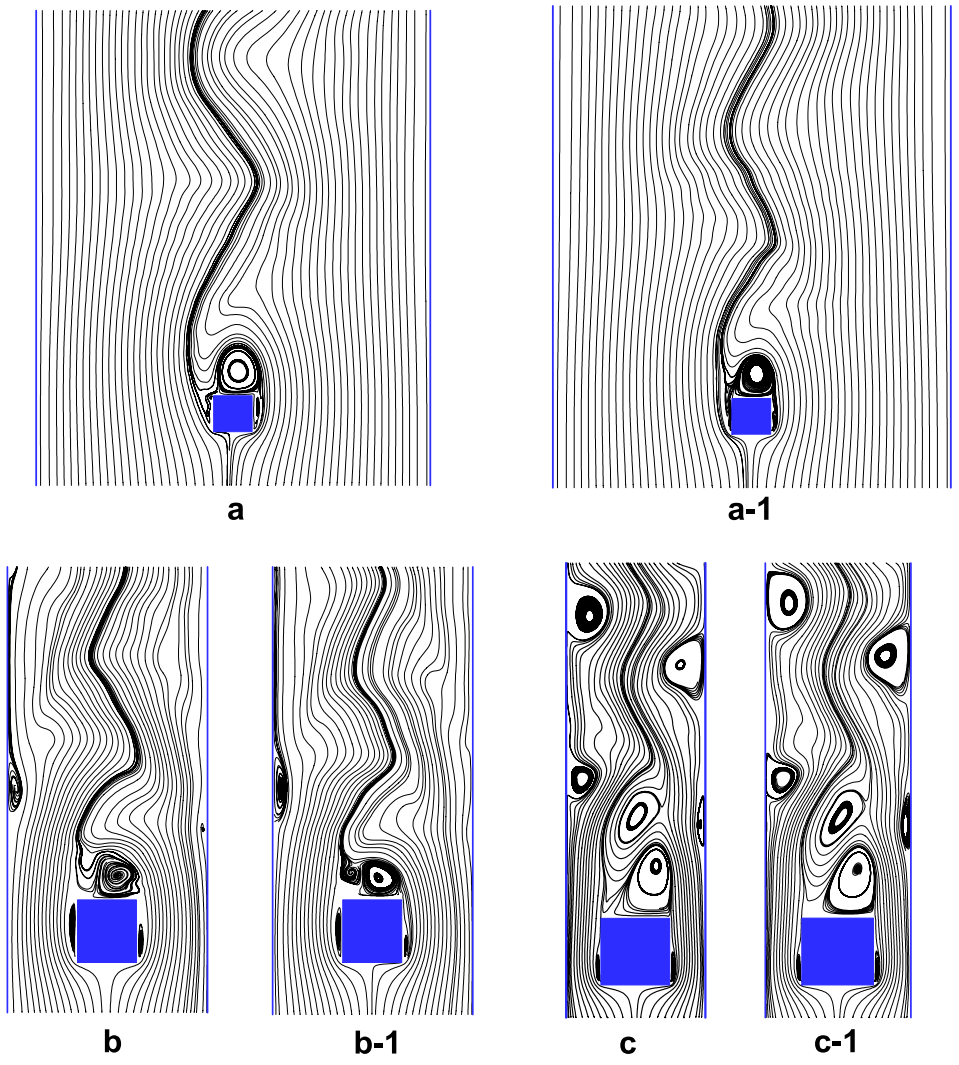


Fig. 7. Instantaneous stream patterns for different blockage ratios $B/H$, under aiding and opposing buoyancy at $Re = 5000$ in a vertical channel: (a) $B/H = 10\%$, $Ri = 1.0$, (a-1) $B/H = 10\%$, $Ri = -1.0$; (b) $B/H = 30\%$, $Ri = 1.0$, (b-1) $B/H = 30\%$, $Ri = -1.0$; (c) $B/H = 50\%$, $Ri = 1.0$, (c-1) $B/H = 50\%$, $Ri = -1.0$.

### 4.4. Vortex shedding and enhancement of heat transfer

The vortex shedding processes under the aiding buoyancy are demonstrated in Fig. 11 while under the opposing buoyancy in Fig. 12, where we plot a sequence of instantaneous streamlines with $B/H = 10\%$ during the flow cycle at $Re = 5000$. One period of the vortex shedding process from dimensionless time is 199.943 to 206.993 for the case of Fig. 11 and 197.807 to 203.607 for the case of Fig. 12. This process demonstrates the event that commences with the shedding of a vortex from the leading tip and ends with the shedding of the next vortex from the same point. For the aiding and opposing buoyancy, the oscillatory nature of the wake above the top surface of the cylinder is similar, but the opposing buoyancy produces a shorter length of the wave flow than the aiding buoyancy in the vertical channel. Thus, the opposing buoyancy results in a smaller re-circulating zone in the wake region than the aiding buoyancy. The influence of buoyancy effect and blockage ratio ($B/H$) of the square cylinder on the lift coefficient $C_L$ and Strouhal number $Sr$ is investigated by indicating the variations of $C_L$ in Fig. 13 and $Sr$ in Table 2. The Strouhal number is defined by

$$Sr = B \cdot f_S / v_\infty \tag{7}$$

In Fig. 13a, the amplitude of temporal variation in $C_L$ increases with increasing $Ri$, but the frequency is bigger at $Ri = -1$ than at $Ri = 1$. The results about the oscillatory motion also can be observed in Figs. 11 and 12. The amplitude and frequency of temporal variation in $C_L$ are almost the same for different $Ri$ values in Fig. 13b and c; in other words, the buoyancy effect on the oscillatory motion is not obvious at $B/H = 30\%$ and 50%. From the profiles of $C_L$ shown in Fig. 13c, the oscillatory variation of lift coefficient begins earlier while $Ri$ increase.

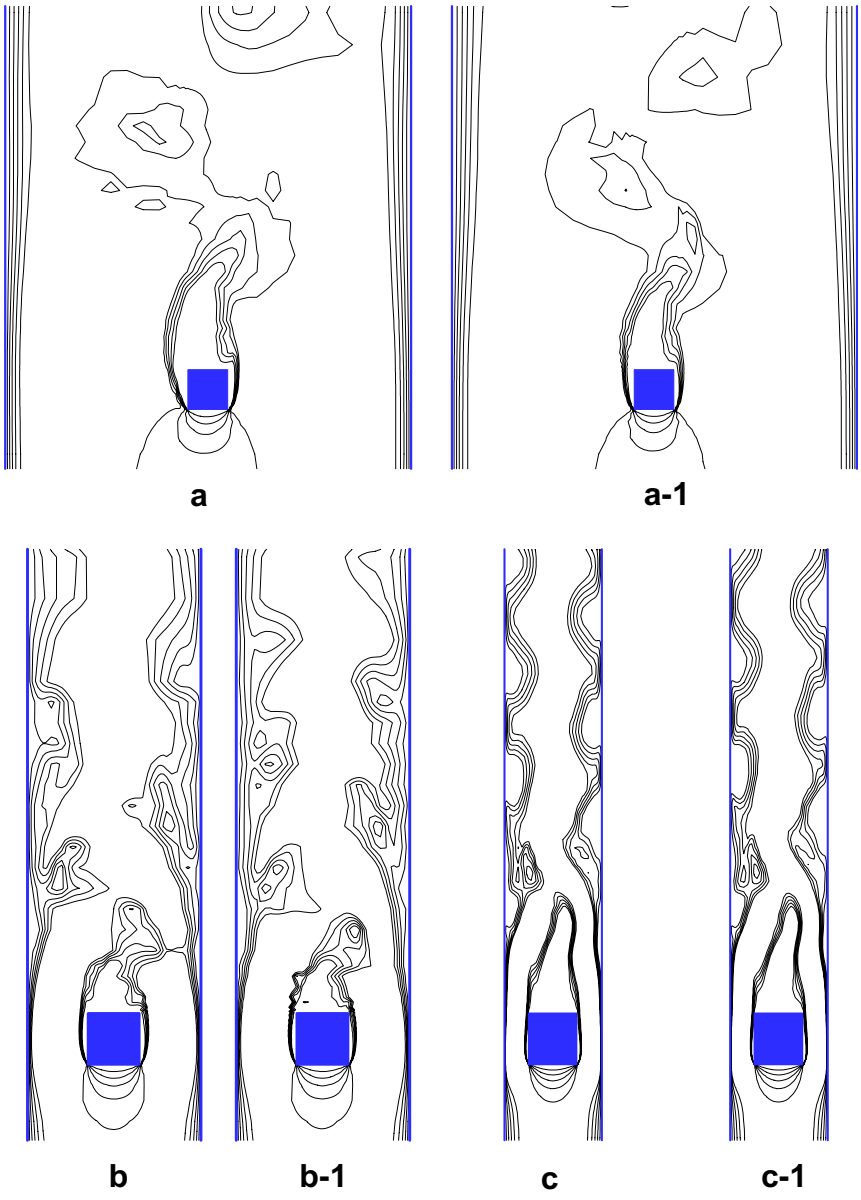


Fig. 8. Instantaneous isotherms for different blockage ratios $B/H$, under aiding and opposing buoyancy at $Re = 5000$ in a vertical channel: (a) $B/H = 10\%$, $Ri = 1$, (a-1) $B/H = 10\%$, $Ri = -1$; (b) $B/H = 30\%$, $Ri = 1$, (b-1) $B/H = 30\%$, $Ri = -1$; (c) $B/H = 50\%$, $Ri = 1$, (c-1) $B/H = 50\%$, $Ri = -1$.

Besides, the wave flows ceases during a long time (about dimensionless time 200–250) while the blockage ratio equals 50%, because the degree of the channel-confinement is enough to cease the oscillation. In Table 2, Strouhal number $Sr$ is bigger for the opposing buoyancy than for the aiding buoyancy at $B/H = 10\%$. For $B/H = 30\%$ and 50%, the relative variation of $Sr$ is smaller for various $Ri$ values. On the other hand, the buoyancy effect on Strouhal number is not obvious at $B/H = 30\%$ and 50%. Besides, Strouhal number increases with increasing blockage ratio $B/H$. Thus, the channel-confinement effect on Strouhal number is obvious for different $Ri$ values. Strouhal number listed in Table 2 is 0.1368 – 0.1724 for $B/H = 10\%$, 0.3454 – 0.4301 for $B/H = 30\%$, and 0.4301 –0.4975 for $B/H = 50\%$. For $Ri = 0$, similar observations have been seen in an experimental study conducted by Okajima [29].

We may investigate the effect of buoyancy and channel-confinement on the heat transfer enhancement by means of the values of the average time-mean Nusselt number for the square cylinder surfaces as follows. The average time-mean Nusselt number is calculated by the values of the time-mean Nusselt number on all node points of each surface. The values of average time-mean Nusselt number on each surface are listed in Table 3 for various $B/H$ values of the cylinder as the $Ri$ value changes at a fixed value of $Re$ (=5000). The value of average time-mean Nusselt number increases with increasing blockage ratio for the cylinder

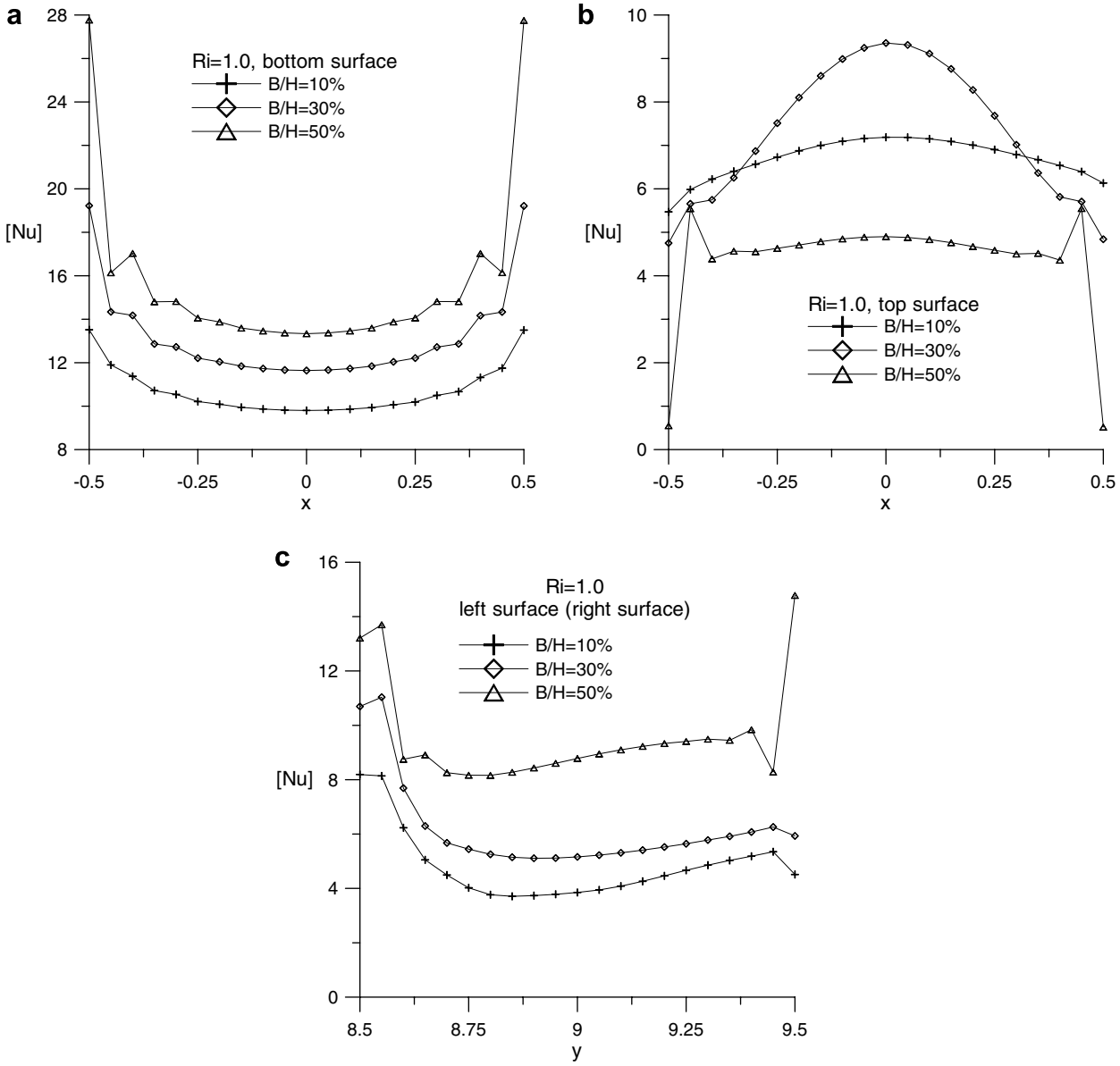


Fig. 9. Time-mean Nusselt number profiles along (a) bottom, (b) top and (c) left (right) surfaces of the square cylinder for different $B/H$ values under aiding buoyancy ($Ri = 1$).

and its faces, except on the top surface. The minimum value of average time-mean Nusselt number exists along the top surface at $B/H = 50\%$. The maximum value of average time-mean Nusselt number for the whole cylinder appears at the blockage ratio $B/H = 50\%$ with $Ri = -1$. As also shown in the italic font in Table 3, the maximum increase in the overall average time-mean Nusselt number is 49.91% at $B/H = 50\%$ with $Ri = -0.25$, but the minimum increase is 19.00% when the blockage ratio $B/H$ is 30% with $Ri = -1$. In all cases, the maximum increase for the overall average $Nu$ is 98.62% at $B/H = 50\%$ and $Ri = 0.5$ on the side surfaces, and the maximum decrease is $-34.87\%$ at $B/H = 50\%$ and $Ri = 1$ on the top surface; this result is mainly caused by the confinement between the channel wall and the cylinder. The channel-confinement improves the heat transfer the best on the side surfaces but impairs it the worst on the top surface, because the velocity of the fluid emanating from the gap between the side faces of the cylinder and the channel wall increases most for $B/H = 50\%$. Besides, the flow jets upward into the wake cavity and causes the most poor heat transfer along the top surface.

## 5. Conclusions

A numerical study of the turbulent flow and heat transfer around a square cylinder with a constant temperature has been systematically performed in a vertical channel under aiding and opposing buoyancy. The main

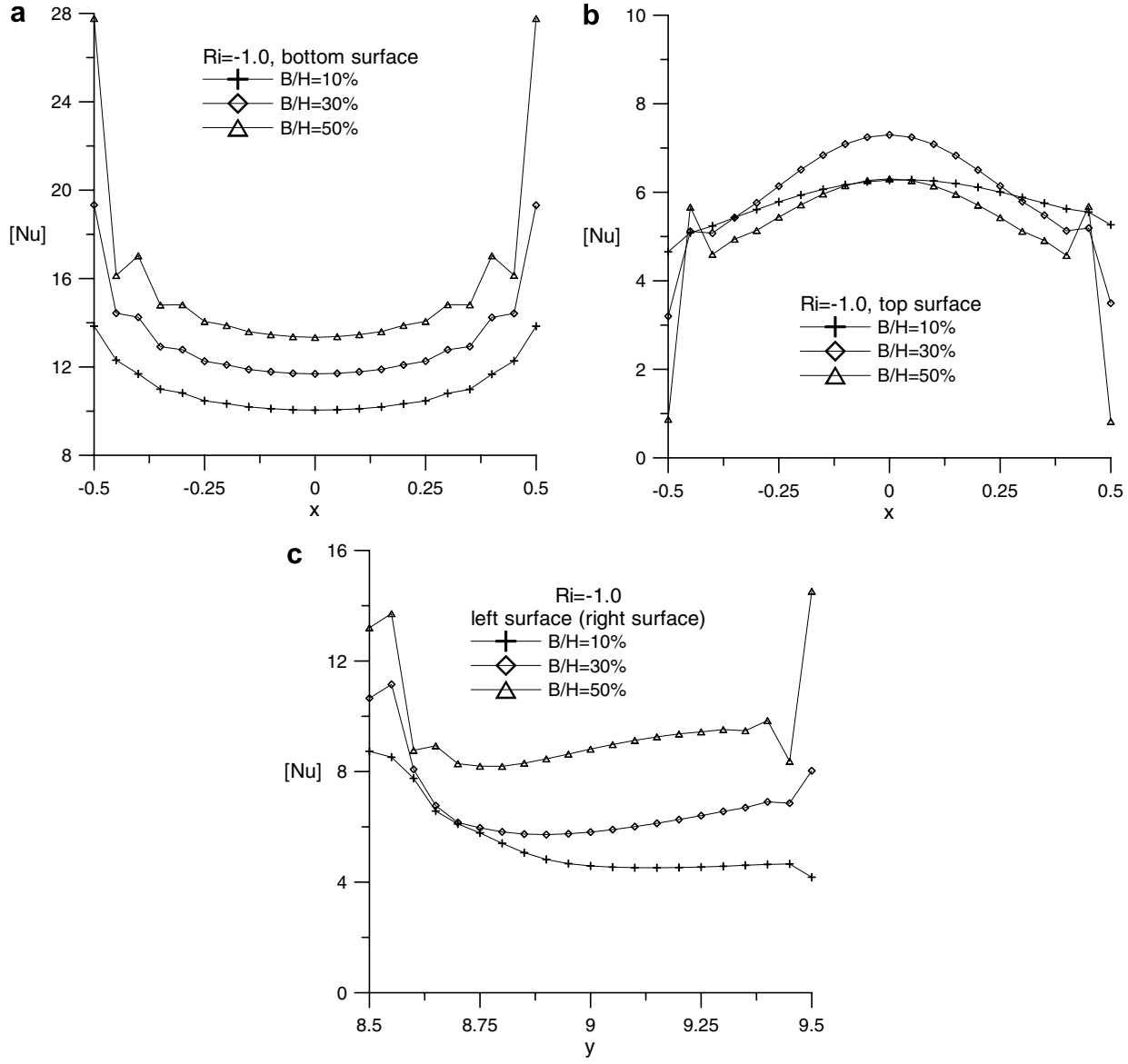


Fig. 10. Time-mean Nusselt number profiles along (a) bottom, (b) top and (c) left (right) surfaces of the square cylinder for different $B/H$ values under aiding buoyancy ($Ri = -1$).

conclusions emerging from the results and discussion are summarized as follows:

(1) The results of normalized Nusselt number computed in this paper are in good agreement with available measurements of Lockett.
(2) At $B/H = 10\%$ and 30%, the influence of aiding buoyancy is prominent on the top surface of the square cylinder, and opposing for the other three surfaces. At $B/H = 50\%$, the buoyancy effect on the local Nusselt number along the bottom and side surfaces is almost in vain.
(3) At $B/H = 10\%$ and 30%, the opposing buoyancy has a shorter length of the wave flow induced by vortex shedding across the square cylinder than the aiding buoyancy in the vertical channel. At $B/H = 50\%$, the buoyancy effect on the turbulent flow can be neglected.
(4) The cylinder Nusselt number increases with increasing blockage ratio for $Ri$ values. The turbulent heat transfer across the square cylinder can be improved by increasing the degree of the confinement between the channel wall and the square cylinder.
(5) When $B/H = 50\%$, the channel-confinement improves the heat transfer the best on the side surfaces but impairs it the worst on the top surface, because of the influence of the jet flow on the side and top surfaces.
(6) At $B/H = 10\%$, the time-dependent turbulent flow motion is only noticeable near the square cylinder

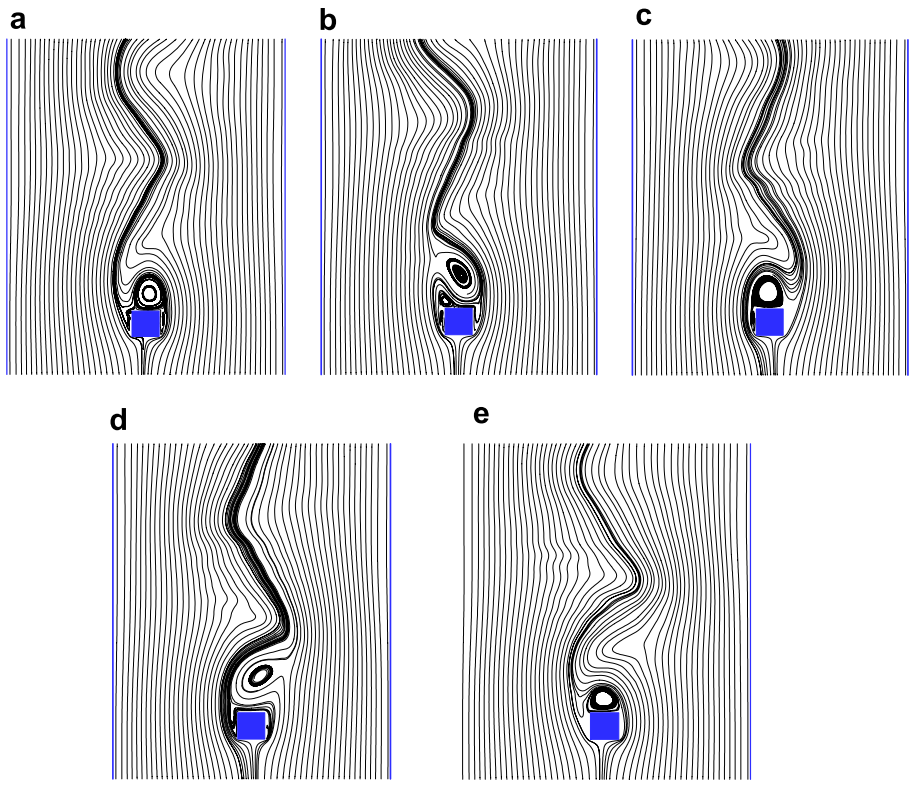


Fig. 11. Sequence of streamlines for the square cylinder under aiding buoyancy ($Ri = 1$) during one cycle at (a) $t = 199.943$, (b) $t = 201.527$, (c) $t = 203.596$, (d) $t = 205.331$ and (e) $t = 206.993$ for $B/H = 10\%$ and $Re = 5000$.

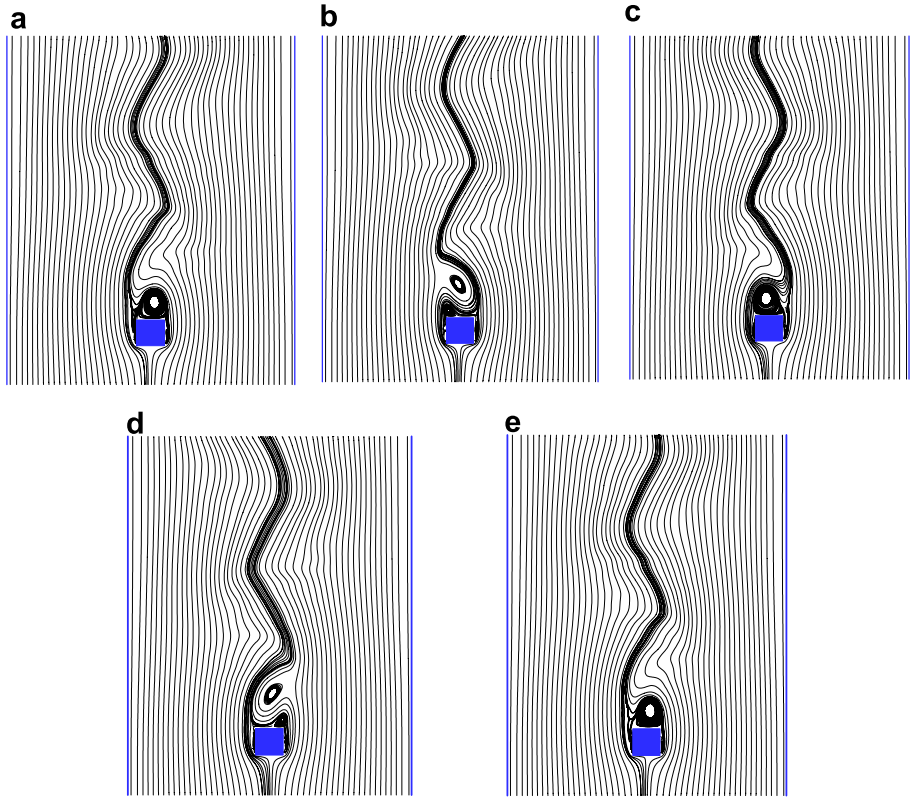


Fig. 12. Sequence of streamlines for the square cylinder under opposing buoyancy ($Ri = -1$) during one cycle at (a) $t = 197.807$, (b) $t = 199.266$, (c) $t = 200.715$, (d) $t = 202.181$ and (e) $t = 203.607$ for $B/H = 10\%$ and $Re = 5000$.

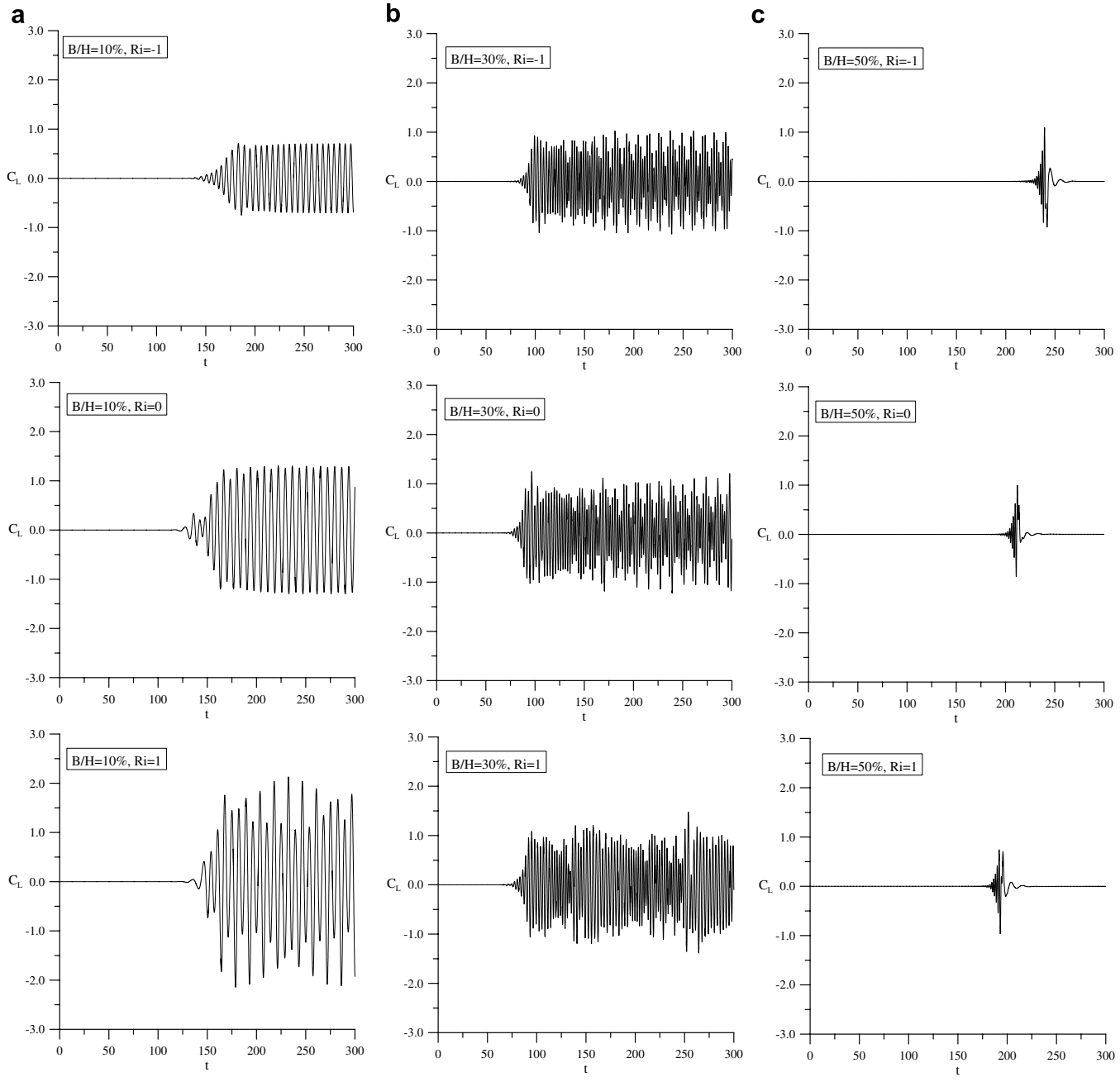


Fig. 13. Lift coefficient $C_L$ vs time for the square cylinder at $Ri = -1$, 0 and 1 with different $B/H$ values. (a) $B/H = 10\%$, (b) $B/H = 30\%$ and (c) $B/H = 50\%$.

and the fluid flow along the channel wall changes nothing. While the blockage ratio increases to be 30% and 50%, the flow along the channel wall becomes unsteady and some re-circulating zones generate along the channel wall.

(7) The vortex shedding across the square cylinder is influenced by the confinement between the channel wall and the square cylinder. The Strouhal number increases with increasing blockage ratio.

(8) For various $Ri$ values, the maximum increase in the overall average time-mean Nusselt number is 49.91% when the blockage ratio $B/H$ is 50% with

Table 2
Strouhal number ($Sr$) for various $B/H$ and $Ri$ values at $Re = 5000$

| $B/H = 10\%$ | | $B/H = 30\%$ | | $B/H = 50\%$ | |
|---|---|---|---|---|---|
| $Ri$ | $Sr$ | $Ri$ | $Sr$ | $Ri$ | $Sr$ |
| 1.00 | 0.1418 | 1.00 | 0.4301 | 1.00 | 0.4635 |
| 0.75 | 0.1431 | 0.75 | 0.4082 | 0.75 | 0.4872 |
| 0.50 | 0.1368 | 0.50 | 0.3578 | 0.50 | 0.4396 |
| 0.25 | 0.1387 | 0.25 | 0.3546 | 0.25 | 0.4975 |
| 0.00 | 0.1422 | 0.00 | 0.3745 | 0.00 | 0.4944 |
| −0.25 | 0.1555 | −0.25 | 0.3802 | −0.25 | 0.4320 |
| −0.50 | 0.1626 | −0.50 | 0.3454 | −0.50 | 0.4808 |
| −0.75 | 0.1692 | −0.75 | 0.3766 | −0.75 | 0.4773 |
| −1.00 | 0.1724 | −1.00 | 0.3883 | −1.00 | 0.4301 |

Table 3
For three $B/H$ values at $Re = 5000$, values of average time-mean Nusselt number along the surfaces of the square cylinder with different $Ri$

| | $Ri = 1.0$ | $Ri = 0.75$ | $Ri = 0.5$ | $Ri = 0.25$ | $Ri = 0$ | $Ri = -0.25$ | $Ri = -0.5$ | $Ri = -0.75$ | $Ri = -1$ |
|---|---|---|---|---|---|---|---|---|---|
| $B/H = 10\%$ | | | | | | | | | |
| Bottom surface | 10.7317 | 10.7534 | 10.7785 | 10.8171 | 10.8556 | 10.9169 | 10.9612 | 10.9980 | 11.0281 |
| Top surface | 6.6928 | 6.3473 | 6.3278 | 5.8921 | 5.7818 | 5.5880 | 5.4247 | 5.1939 | 5.7818 |
| Left (right) surface | 4.8249 | 4.9087 | 4.8227 | 4.9208 | 4.9156 | 5.0151 | 5.1179 | 5.2449 | 5.3971 |
| Overall | 6.7686 | 6.7295 | 6.6879 | 6.6377 | 6.6171 | 6.6338 | 6.6554 | 6.6704 | 6.9010 |
| $B/H = 30\%$ | | | | | | | | | |
| Bottom surface | 13.2019 | 13.2326 | 13.2251 | 13.2335 | 13.2376 | 13.2421 | 13.2476 | 13.2560 | 13.2637 |
| | *23.02%* | *23.06%* | *22.70%* | *22.34%* | *21.94%* | *21.30%* | *20.86%* | *20.53%* | *20.27%* |
| Top surface | 7.3313 | 5.9855 | 5.9846 | 6.2200 | 6.4619 | 6.2914 | 6.1745 | 6.4254 | 5.9330 |
| | *9.54%* | *−5.70%* | *−5.42%* | *5.57%* | *11.76%* | *12.59%* | *13.82%* | *23.71%* | *2.62%* |
| Left (right) surface | 6.1757 | 6.6459 | 6.5292 | 6.6877 | 6.6664 | 6.6881 | 6.7393 | 6.7962 | 6.8266 |
| | *28.00%* | *35.39%* | *35.38%* | *35.91%* | *35.62%* | *33.36%* | *31.68%* | *29.58%* | *26.49%* |
| Overall | 8.2212 | 8.1275 | 8.0670 | 8.2072 | 8.2581 | 8.2274 | 8.2252 | 8.3184 | 8.2125 |
| | *21.46%* | *20.77%* | *20.62%* | *23.65%* | *24.80%* | *24.02%* | *23.59%* | *24.71%* | *19.00%* |
| $B/H = 50\%$ | | | | | | | | | |
| Bottom surface | 15.7689 | 15.7694 | 15.7697 | 15.7703 | 15.7708 | 15.7710 | 15.7716 | 15.7720 | 15.7721 |
| | *46.94%* | *46.65%* | *46.31%* | *45.79%* | *45.28%* | *44.46%* | *43.89%* | *43.41%* | *43.02%* |
| Top surface | 4.3592 | 4.3136 | 4.5649 | 4.3360 | 4.3706 | 4.8308 | 4.4723 | 4.5236 | 5.1269 |
| | *−34.87%* | *−32.04%* | *−27.86%* | *−26.41%* | *−24.41%* | *−13.55%* | *−17.56%* | *−12.91%* | *−11.33%* |
| Left (right) surface | 9.5768 | 9.5832 | 9.5789 | 9.5906 | 9.5944 | 9.5879 | 9.6004 | 9.6016 | 9.5907 |
| | *98.49%* | *95.23%* | *98.62%* | *94.90%* | *95.18%* | *91.18%* | *87.58%* | *83.07%* | *77.70%* |
| Overall | 9.8204 | 9.8124 | 9.8731 | 9.8219 | 9.8326 | 9.9444 | 9.8612 | 9.8747 | 10.0201 |
| | *45.09%* | *45.81%* | *47.63%* | *47.97%* | *48.59%* | *49.91%* | *48.17%* | *48.04%* | *45.20%* |

*Note:* Values in the italic font designating the percentage change relative to the $B/H = 10\%$ cases.

$Ri = -0.25$; the minimum increase is 19.00% when the blockage ratio $B/H$ is 30% with $Ri = -1$.

## Acknowledgement

The authors gratefully acknowledge the partial financial support of this project by the National Council of the Republic of China.

## References

[1] C.H.K. Williamson, Vortex dynamics in the cylinder wake, Ann. Rev. Fluid Mech. 28 (1996) 477–539.
[2] M.M. Zdravkovich, Flow Around Circular Cylinders, Fundamentals, vol. 1, Oxford University Press, New York, 1997.
[3] J.L. Rosales, A. Ortega, J.A.C. Humphrey, A numerical investigation of the convection heat transfer in unsteady laminar flow past a single and tandem pair of square cylinders in a channel, Numer. Heat Transfer A 38 (2000) 443–465.
[4] R.J. Yang, L.M. Fu, Thermal and flow analysis of a heated electronic component, Int. J. Heat Mass Transfer 44 (2001) 2261–2275.
[5] S. Turki, H. Abbassi, S.B. Nasrallah, Two-dimensional laminar fluid flow and heat transfer in a channel with a built-in square cylinder, Int. J. Therm. Sci. 42 (2003) 1105–1113.
[6] M. Rahbana, H. Hadi-Moghaddam, Numerical investigation of convection heat transfer in unsteady laminar flow over a square cylinder in a channel, Heat Transfer Eng. 26 (10) (2005) 21–29.
[7] A. Valencia, Turbulent flow and heat transfer in a channel with a square bar detached from the wall, Numer. Heat Transfer A 37 (2000) 289–306.
[8] K.S. Chang, J.Y. Sa, The effect of vortex shedding in the near wake of a circular cylinder, J. Fluid Mech. 220 (1990) 253–266.
[9] A. Sharma, V. Eswaran, Effect of channel-confinement and aiding/opposing buoyancy on the two-dimensional laminar flow and heat transfer across a square cylinder, Int. J. Heat Mass Transfer 48 (2005) 5310–5322.
[10] C.J. Ho, M.S. Wu, J.B. Jou, Analysis of buoyancy-aided convection heat transfer from a horizontal cylinder in a vertical duct at low Reynolds number, Wärme. Stoffübertrag. 25 (1990) 337–343.
[11] C. Fureby, G. Tabor, H.G. Weller, A.D. Gosman, A comparative study of subgrid scale models in homogeneous isotropic turbulence, Phys. Fluids 9 (5) (1997) 1416–1429.
[12] S. Sakamoto, S. Murakami, A. Mochida, Numerical study on flow past 2D square cylinder by large eddy simulation: comparison between 2D and 3D computations, J. Wind Eng. Ind. Aerod. 50 (1993) 61–68.
[13] J.P. Van Doormaal, G.D. Raithby, Enhancements of the SIMPLE method for predicting incompressible fluid flows, Num. Heat Trans. 7 (1984) 147–163.
[14] B. Galperin, S. Orszag, Large Eddy Simulation of Complex Engineering and Geophysical Flows, Cambridge University Press, Cambridge, 1993, pp. 231–346.
[15] G.B. Deng, J. Piquet, P. Queutey, M. Visonneau, A new fully coupled solution of the Navier–Stokes equations, Int. J. Numer. Meth. Fluids 19 (1994) 605–639.
[16] Y.Y. Tsui, A study of upstream weighted high-order differencing for approximation to flow convection, Int. J. Numer. Meth. Fluids 13 (1991) 167–199.
[17] D. Kershaw, The incomplete Cholesky-conjugate gradient method for the iterative solution of systems of linear equations, J. Comput. Phys. 26 (1978) 43–65.
[18] H. Van Der Vorst, BI-CGSTAB: a fast and smoothly converging variant of BI-CG for the solution of nonsymmetric linear system, SIAM J. Sci. Stat. Comput. 13 (2) (1992) 631–644.
[19] S. Habchi, S. Acharya, Laminar mixed convection in a partially blocked vertical channel, Int. J. Heat Mass Transfer 29 (1986) 1711–1722.

[20] A. Yoshizawa, K. Horiuti, Statistically-derived subgrid-scale kinetic energy model for the large-eddy simulation of turbulent flows, J. Phys. Soc. Jpn. 54 (8) (1985) 2834–2839.
[21] A.W. Verman, B.J. Geurts, J.G.M. Kuerten, P.J. Zandbergen, A finite volume approach to large eddy simulation of compressible, homogeneous isotropic, decaying turbulence, Int. J. Numer. Meth. Fluids 15 (1992) 799–816.
[22] J. Smagorinsky, General circulation experiments with the primitive equations, Mon. Weather Rev. 91 (1963) 99–164.
[23] U. Piomelli, High Reynolds number calculations using the dynamic subgrid scale stress model, Phys. Fluids A 5 (6) (1993) 1484–1490.
[24] H. Werner, H. Wengle, Large-eddy simulation of the flow over a square rib in a channel, in: Proceedings of the Seventh Symposium Turbulent Shear Flows, Stanford University, 1989, pp. 10.2.1–10.2.6.
[25] C.L.V. Jayatilleke, The influence of Prandtl number and surface roughness on the resistance of the laminar sublayer to momentum and heat transfer, Prog. Heat Mass Transfer 1 (1969) 193–329.
[26] J.F. Lockett, Heat transfer from roughened surfaces using laser interferometers, Ph.D. Thesis, Department of Mechanical Engineering, The City University, London, 1987.
[27] M. Ciofalo, M.W. Collins, Large-eddy simulation of turbulent flow and heat transfer in plane and rib-roughened channels, Int. J. Numer. Meth. Fluids 15 (1992) 453–489.
[28] S.Y. Kim, H.J. Sung, J.M. Hyun, Mixed convection from multiple-layered boards with cross-streamwise periodic boundary conditions, Int. J. Heat Mass Transfer 35 (11) (1992) 2941–2952.
[29] A. Okajima, Strouhal numbers of rectangular cylinders, J. Fluid Mech. 123 (1982) 379–398.